Thermal equilibrium of pure electron plasmas across a central region of magnetic surfaces

Michael Hahn and Thomas Sunn Pedersen
*Department of Applied Physics and Applied Mathematics, Columbia University,
New York, New York 10027, USA*

Measurements of the equilibria of plasmas created by emission from a biased filament located off the magnetic axis in the Columbia Non-neutral Torus (CNT) [T. S. Pedersen, J. P. Kremer, R. G. Lefrancois *et al.*, Fusion Sci. Technol. **50**, 372 (2006)] show that such plasmas have equilibrium properties consistent with the inner surfaces being in a state of cross-surface thermal equilibrium. Numerical solutions to the equilibrium equation were used to fit the experimental data and demonstrate consistency with cross-surface thermal equilibrium. Previous experiments in CNT showed that constant temperatures across magnetic surfaces are characteristic of CNT plasmas, implying thermal confinement times much less than particle confinement times. These results show that when emitting off axis there is a volume of inner surfaces where diffusion into that region is balanced by outward transport, producing a Boltzmann distribution of electrons. When combined with the low thermal energy confinement time this is a cross-surface thermal equilibrium. © *2009 American Institute of Physics*. [DOI: 10.1063/1.3158948]

I. INTRODUCTION

The equilibrium of pure electron plasmas has been studied extensively in Penning traps, which can have essentially infinite confinement times and relax to global thermal equilibrium.[1] This is possible because conservation of canonical angular momentum allows the electrons to come to thermal equilibrium with each other but still be confined magnetically.[2–5]

The Columbia Non-neutral Torus (CNT)[6] is a stellarator being used to study non-neutral plasmas on magnetic surfaces. The transport along the field lines is very fast so the plasma is in thermal equilibrium on each magnetic surface, but there is not necessarily thermal equilibrium across the surfaces.[7] In this paper we present results showing that a volume of inner magnetic surface can relax to a cross-surface thermal equilibrium. The thermal equilibrium is like the one produced in Penning traps by an equipotential cathode.[8]

The relaxation to cross-surface thermal equilibrium depends on inward transport of electrons across the magnetic surfaces, which balances the outward transport. In studies of pure electron plasmas on magnetic surfaces in the compact helical system (CHS)[9,10] experiment the electrons were injected from outside the last closed flux surface and were transported across the magnetic surfaces to fill the plasma.[9–12] This was done using an electron gun to give the electrons a large kinetic energy and formed a plasma with a central plasma potential comparable to the injection energy. In contrast, in CNT the plasma is created using a heated biased filament inside the surfaces. These electrons are born with very low kinetic energy, but overcome the potential barrier so that inward transport and thermal equilibrium are observed. We find that there are some significant differences between the equilibria created using these methods.

Typical plasmas in CNT are formed by emitting from a filament placed on the magnetic axis. Electrons diffuse outward from the axis filling the plasma.[13] In this paper we will present experimental measurements of the equilibrium and confinement properties of pure electron plasmas created from emission away from the magnetic axis. The radial equilibrium profiles will be compared with numerical equilibrium reconstructions and analytic equilibria in a simplified geometry.

II. THEORY

We begin by considering several possible ways the electron density could be arranged when emitting off axis. We consider a zero temperature plasma, a plasma where transport is purely diffusive across the surfaces inside the surface where the emitter is located and thermal equilibrium across the inner surfaces. The first two possibilities are physically unrealistic, but the last case, cross-surface thermal equilibrium, is a physically reasonable model.

In a cold plasma with $T_e = 0$ the electrons do not have enough energy to enter the surfaces inside the location of the emitter. If there are no electrons on the inner surfaces the plasma potential on the inner surfaces is the same as the potential on the surface of the emitter Φ_0. Even a small density, δn_e, present on the inner surfaces would make the plasma potential more negative than Φ_0, preventing electrons from entering that region. Therefore the density on the inner surfaces in the zero temperature case must be $n_e = 0$. The corresponding plasma potential across the inner surfaces is $\Phi = \Phi_0$.

Another simplified model for off-axis equilibrium is to neglect the electrostatic potential hill for the electrons and assume that the density on the inner surfaces is determined only by diffusion. Diffusion acts to smooth out any peaks and troughs in the density distribution of the electrons, so in the absence of internal sources the density across the inner

surfaces will be a constant ($\nabla n_e = 0$). The density will be the same as the density on the boundary, i.e., the surface where the emitter is located, $n_e = n_{e,0}$.

The plasma potential in this purely diffusive model can be illustrated by considering a cylindrical geometry. Poisson's equation can be solved in a cylindrical geometry subject to the boundary conditions that the plasma potential at location of the emitter is continuous $\Phi = \Phi_0$ at $r = r_0$ and there is no gradient at the origin $d\Phi/dr = 0$ at $r = 0$. The solution is parabolic in r with the potential more negative at the axis than Φ_0 by a factor proportional to r_0 and n_0, $\Phi(r) = \Phi_0 - e n_{e,0}/4\epsilon_0 (r_0^2 - r^2)$.

When emitting from an off-axis emitter there is transport into the inner surfaces from the emitter and also transport out from the inner surfaces. When the inward and outward transports are balanced the plasma is in equilibrium. If the electron plasma comes into thermal equilibrium the electrons follow a Boltzmann distribution $n \sim \exp(e\Phi/T_e)$, where Φ must be determined self-consistently with the electron density. When the kinetic energy transport is also balanced so that T_e is constant across the inner surfaces, which is almost always the case experimentally, this situation represents a thermal equilibrium across the magnetic surfaces.

Some qualitative properties of cross-surface thermal equilibrium can be identified using a simple analytical model. The equilibrium equation for a pure electron plasma on magnetic surfaces assumes that rapid transport along the field lines establishes thermal equilibrium on each surface,[7]

$$\nabla^2 \Phi = \frac{e}{\epsilon_0} N(\Psi) \exp\left(\frac{e\Phi}{T_e(\Psi)}\right). \tag{1}$$

Surfaces are labeled by the coordinate Ψ. $T_e(\Psi)$ and $N(\Psi)$ are constant on a magnetic surface, but the density n_e and potential Φ are functions of all three coordinates. Suppose there is a surface Ψ_0 so that for $\Psi < \Psi_0$ $N(\Psi) = N_0$ and $T_e(\Psi) = T_{e,0}$ are constants, in other words those surfaces are in cross-surface thermal equilibrium. In contrast with the purely diffusive case $N(\Psi)$ is a constant instead of $n_e = N(\Psi)\exp(e\Phi/T_e)$. Then in that region

$$\nabla^2 \Phi = \frac{e}{\epsilon_0} N_0 \exp\left(\frac{e\Phi}{T_{e,0}}\right). \tag{2}$$

Equation (2) was presented as an extension of Eq. (1), which comes from the fluid equations and parallel force balance. In this case, the magnetic surfaces do not affect the equilibrium state, although they may effect the relaxation rate to reach that equilibrium. Thermal equilibrium is established across the magnetic surfaces in addition to along the field lines. A thermodynamic equilibrium in an electric potential is characterized by a constant temperature and a Boltzmann distribution of electrons.[14] This is a general result that also applies to systems other than plasmas, such as solutions of electrolytes.[15,16] The solutions to the Poisson–Boltzmann equation may be used to calculate thermodynamic quantities, in particular the Helmholtz free energy.[17]

A boundary condition on Eq. (2) is that the solutions to Eq. (1) for $\Psi > \Psi_0$ and Eq. (2) must match at $\Psi = \Psi_0$. Continuity in temperature and density requires that $T_{e,0} = T_e(\Psi_0)$

and $N_0 = N(\Psi_0)$. To simplify the boundary conditions on the thermal equilibrium region define $\Phi_<$ to satisfy

$$\Phi(\Psi < \Psi_0) = \Phi_< + \Phi_0, \tag{3}$$

where $\Phi_0 \equiv \Phi(\Psi_0)$. In general the magnetic surfaces are not equipotentials so Φ_0 and $\Phi_<$ will be functions of toroidal and poloidal (ϕ and θ) angles. Inserting the expression into the equilibrium equation (2) for $\Phi_<$, one can identify the term $N_0 \exp(e\Phi_0/T_{e,0})$ as n_0 and the density at Ψ_0, which is also a function of ϕ and θ. The equilibrium for a central region of surfaces in thermal equilibrium is

$$\nabla^2 \Phi_< = \frac{e}{\epsilon_0} n_0 \exp\left(\frac{e\Phi_<}{T_{e,0}}\right), \tag{4}$$

which is subject to the boundary condition $\Phi_< = 0$ at $\Psi = \Psi_0$. The second boundary condition for this second order differential equation is that the radial derivatives vanish at the origin, $\Psi = 0$.

To examine the properties of these equilibria consider a circular cross section, that is, a magnetic field having concentric cylindrical magnetic surfaces. In this approximation the magnetic surface coordinate Ψ is proportional to r, the radius. By cylindrical symmetry the potential $\Phi_<$ becomes a function only of the radius and Φ_0 and n_0 become constants. With these simplifications Eq. (4) can be solved analytically using some substitutions.[18] The equation can be normalized by defining $\tilde{\Phi} \equiv e\Phi_</T_{e,0}$ and $\rho \equiv r/\lambda_{D,0}$ with $\lambda_{D,0}$ the Debye length at Ψ_0 (or r_0) and $\rho_0 \equiv \rho(\Psi_0)$. Then the solution to this Poisson–Boltzmann equation for thermal equilibrium across the inner surfaces of a cylindrical stellarator is given by

$$\tilde{\Phi} = \ln\left(\frac{8}{C\left(1 - \frac{\rho^2}{C}\right)^2}\right), \tag{5}$$

$$C = \rho_0^2 + 4 + 2\sqrt{4 + 2\rho_0^2}. \tag{6}$$

These solutions have some general characteristics. The plasma potential becomes more negative than the potential at the edge of the cross-surface thermal equilibrium region by a few T_e/e (Fig. 1). The magnitude of the drop is a function of the size of the thermal equilibrium region measured in units of the local Debye length at the boundary $\lambda_{D,0}$ (Fig. 2). The density on the inner surfaces is significantly less than the density on the boundary, but is still appreciable. These same properties can be seen in the experimental data that will be presented in Sec. III.

The equilibrium of this cylindrical case is the same as one predicted for Penning traps in which a hollow electron column less than $\sqrt{8}$ central Debye lengths in radius is formed from an equipotential cathode.[8] In the results that follow there must be transport across the magnetic field to allow the plasma to relax to the observed thermal equilibrium.
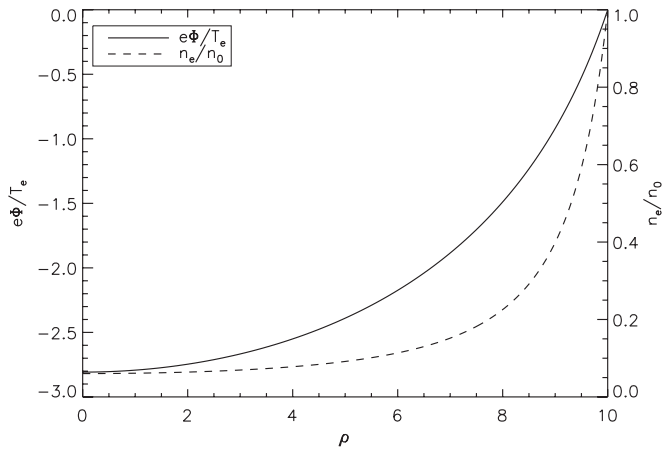
FIG. 1. The solution to the Poisson–Boltzmann equation for a cross-surface thermal equilibrium region in a cylinder is plotted. ρ is the radial distance normalized by the Debye length at the boundary, $\rho \equiv r/\lambda_{D,0}$. The potential drops a few factors of T_e below the potential at the boundary with the bulk plasma. The density at the core is an order of magnitude less than the density of the external plasma. In this plot the region is 10 $\lambda_{D,0}$ in radius.

III. MEASUREMENT TECHNIQUE

The CNT device (Fig. 3) produces magnetic surfaces with average major radius $R=30$ cm and minor radius $a=15$ cm. A high vacuum is needed to keep the ion fraction low, and for the data presented here the vacuum was typically 5×10^{-9} Torr for the conducting boundary data and 2×10^{-8} Torr for the data without the boundary. The reason for the difference is that a leak was closed when the boundary was installed. At these pressures the electron-neutral collision rate, ν_{en}, is $\nu_{en} \approx 25$ s^{-1} or 100 s^{-1}. The plasma is in steady state with the ion creation being balanced by recombination on the insulating rods that hold the probe filaments. The resulting ion fraction is $<1\%$, so these can be considered pure electron plasmas. The electron-electron collision, ν_{ee} rate is roughly an order of magnitude less than the electron-neutral collision rate. The magnetic field strength for equilibrium experiments is usually set to 0.02 T. Larger
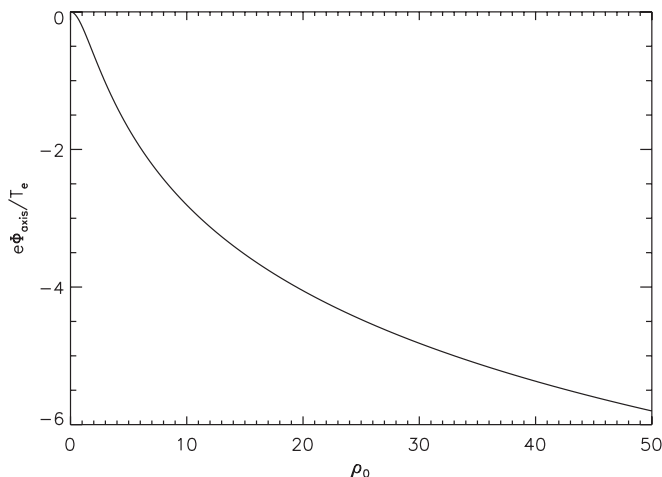

FIG. 2. The analytic solution to the Poisson–Boltzmann equation in a cylinder shows that as radius of the thermal equilibrium region increases and the central potential becomes more negative. Here ρ_0 is the location of the boundary in units of the boundary Debye length, $\lambda_{D,0}$.
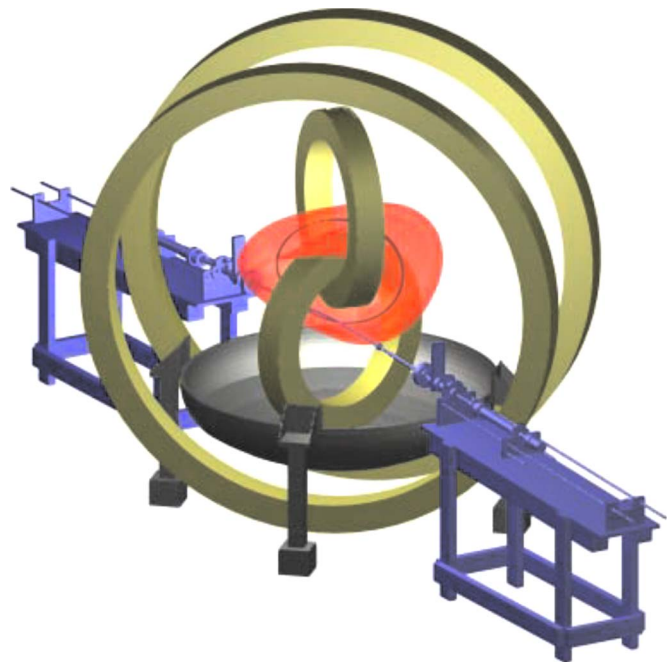

FIG. 3. (Color online) Computer aided design (CAD) drawing of the CNT device showing magnetic field coils, the shape of the magnetic surfaces, and the location of the probe arrays.

magnetic field strengths reduce cross field transport making probe measurements more perturbing and less accurate, while at smaller magnetic field strengths the magnetic surfaces are degraded.[19]

In CNT magnetic surfaces are labeled with the magnetic surface (pseudoradial) coordinate Ψ normalized so that $\Psi=0$ on the magnetic axis and $\Psi=1$ on the last closed flux surface. The shape of the magnetic surfaces varies so that $\Psi=1$ represents a radial distance of between 5.6 cm at the thin cross section to 18 cm at the thick cross section.

Equilibrium properties of the non-neutral plasmas in CNT are measured using internal particle flux probes. These probes can be operated as emissive (hot) probes or Langmuir (cold) probes.[20] The plasma potential, density, and temperature are measured using the techniques outlined in Ref. 20. The uncertainty analysis is done using a Monte Carlo method like the one described in Ref. 21. Density measurements have asymmetric exponential error bars because they depend on the exponential of a measured quantity. The presence of the conducting boundary has also enhanced some systematic effects that lead to an overestimate of the density using this method. However the density can be accurately inferred from the plasma potential measurements using the equilibrium equation (1).

For the experiments reported here probes were located at the thin cross section as shown in Fig. 3. The emitter filament was located on one array and the filaments on the other were used to diagnose the plasma.

When the plasma is in steady state equilibrium the electron loss rate is balanced by the emission current of electrons into the plasma. The confinement time can be calculated by dividing the total electron inventory N_e by the loss rate $\tau = eN_e/I_{emission}$. The electron inventory can be estimated by
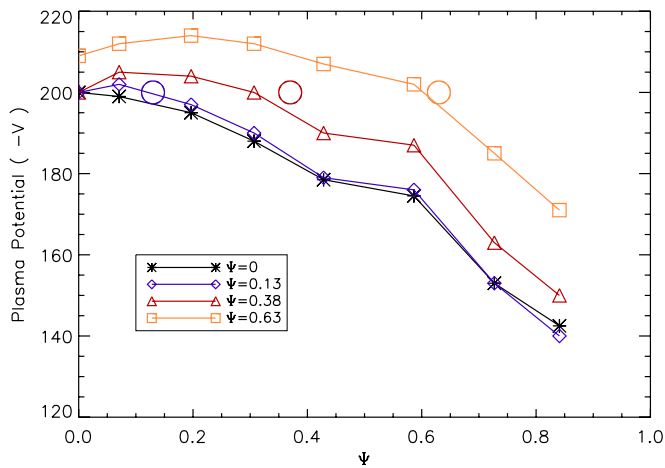
FIG. 4. (Color online) Potential profiles when emitting using a 200 V bias at different off-axis positions for the nonconforming boundary condition. The plasma potential becomes more negative than 200 V on the inner surfaces. The effect is most clear in this figure when the emitter is at $\Psi=0.63$ or $\Psi=0.38$. Circles are centered on the point ($\Psi_{emitter}$, 200 V).

FIG. 6. (Color online) Density profiles when emitting using a 200 V bias at different off-axis positions for the nonconforming boundary condition. A peak in density moves outward as the emitter position is moved outward.

integrating the density from a numerical equilibrium reconstruction.

Experiments were done with two different electrostatic boundary conditions: the original one set by the grounded coils and the vacuum chamber, as described in previous publications,[13,21] and a new flux surface conforming grounded mesh.[22] The latter ensures that the electrostatic potential is zero at the edge of the plasma and can enforce good alignment between the surfaces of constant electrostatic potential and the outer magnetic surfaces.

IV. EXPERIMENTAL RESULTS

For both boundary conditions we observe that the plasma potential becomes more negative than the emitter bias on the inner surfaces, with the potential approaching the emitter bias at the surface of emission (Figs. 4 and 5). This

effect is most pronounced when the emitter is at the furthest radial location measured $\Psi=0.63$, but it is also visible when emitting at the more moderate $\Psi=0.33$ or $\Psi=0.38$. The emission from $\Psi=0.13$ produces potential profiles that are difficult to distinguish from on-axis emission.

The density measurements showed that the density on the inner surfaces is significantly smaller than the density near the location of the emitter, but still appreciable, which is consistent with the potential measurements (Figs. 6 and 7). The Debye length in the core becomes larger so that the plasma has the property $a/\lambda_D \sim 1$, which is a hot plasma. Outside the surface of the emitter there is a higher density cold plasma, $a/\lambda_D \sim 10$.

For the nonconforming boundary condition the temperature profiles when emitting at different radial positions have the same magnitude and flat profiles, within the experimental uncertainties, for much of the plasma independent of emitter
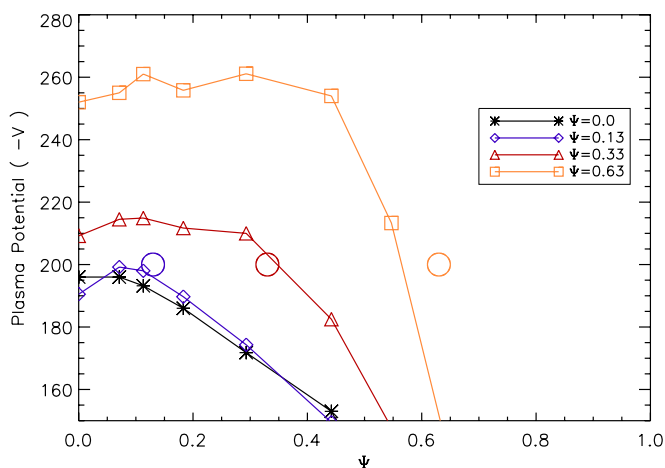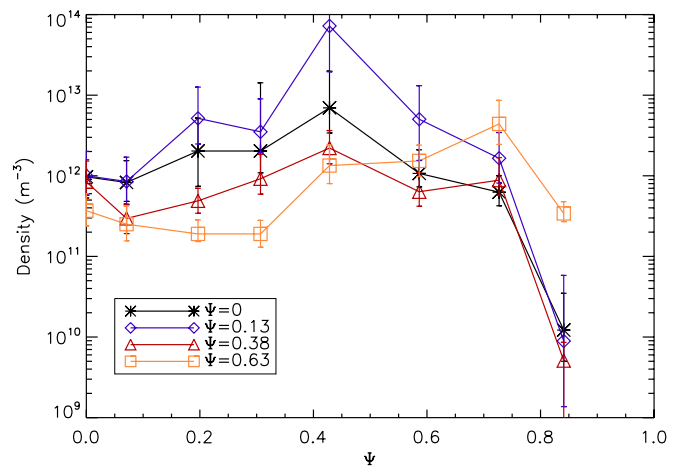

FIG. 5. (Color online) Potential profiles when emitting using a 200 V bias at different off-axis positions with the conforming conducting boundary condition. The plasma potential becomes more negative than 200 V on the inner surfaces by a few T_e. The effect is clear in this figure when the emitter is at $\Psi=0.63$ or $\Psi=0.33$. Circles are centered on the point ($\Psi_{emitter}$, 200 V).
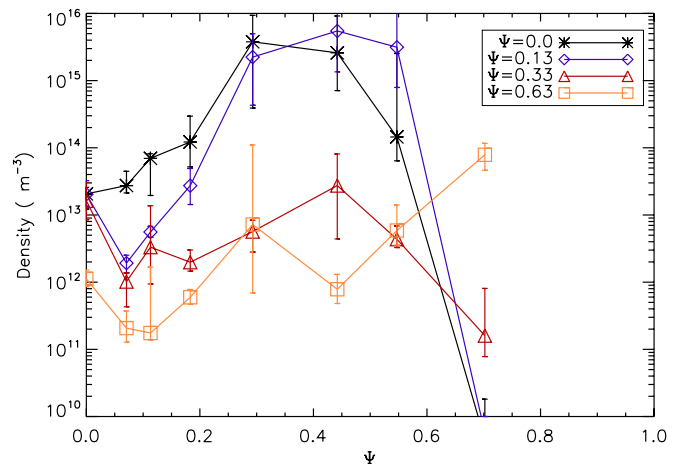

FIG. 7. (Color online) Density profiles when emitting at different off-axis positions with the conforming conducting boundary condition. In this case large errors in the density measurements make a pattern hard to discern, but the measurements are not inconsistent with a density peak moving outward with emitter position. Additionally, since the installation of the conducting boundary there seem to be systematic errors, which have not yet been accounted for in the uncertainty analysis.
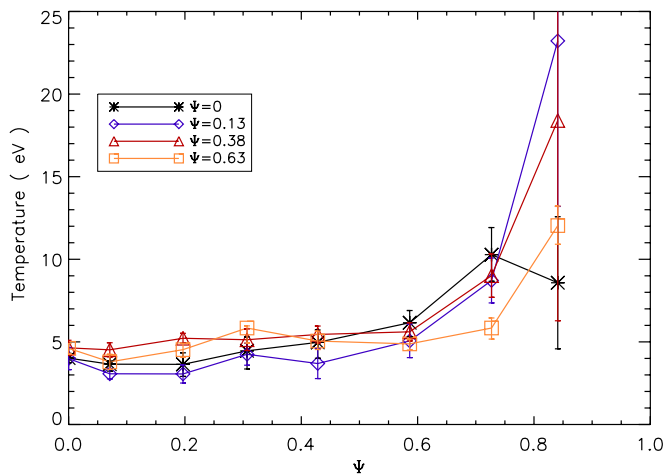
FIG. 8. (Color online) Temperature profiles when emitting using a 200 V bias at different off-axis positions for the nonconforming boundary condition. T_e is about 4 eV for most of the plasma independent of emitter position.

location (Fig. 8). With the conforming boundary the magnitude of the temperature depends significantly on the location of the emitter and is a minimum when the emitter is located on the magnetic axis (Fig. 9). Flat temperature profiles across the inner surfaces persist with the new boundary condition.

In the conforming boundary case the large changes in plasma potential can be explained if the potential drop is some multiple α of the temperature where α depends on emitter position. This is what is expected if the surfaces are in thermal equilibrium with each other. It can be checked experimentally by comparing the difference between the plasma potential inside the location of the emitter and the emitter bias divided in units of the temperature, $\alpha = e(\Phi - V_{em})/T_e$. For an emitter placed at $\Psi = 0.63$ with several different biases, 200, 100, and 73 V, the values of α were 5.6, 5.9, and 5.6, respectively, which is consistent with a potential drop proportional to the temperature. For an emitter at $\Psi = 0.33$ with emitter biases of 200, 167, and 100 V, α was

measured to be 3.0, 1.7, and 3.4, which demonstrates that α increases with displacement of the emitter from the axis.

These results, where the electrons diffuse inward having very little initial kinetic energy, are in contrast with the results of the CHS experiment, where the electrons are injected with a very large initial kinetic energy. The high energy electrons are capable of traveling up the potential barrier formed by the electron plasma. They establish equilibrium with a central potential that is approximately the initial electron energy. For that case the plasma potential is inversely related to the electron temperature because of energy conservation. The plasma potential is also independent of the position of the electron gun, except to the extent that the conducting structure of the electron gun perturbs the plasma.[9,10]

The confinement time for each emitter location was also measured. The total electron inventory was estimated using numerical equilibrium reconstructions. The uncertainty in N_e was estimated from reconstructions that were perturbed from the one that best matched the experimental data.

The confinement times for different emitter positions are recorded in Table I for the nonconforming boundary condition and Table II for measurements with the conforming boundary. The confinement time is insensitive to significant radial displacements of the emitter from the magnetic axis. With the conforming boundary the confinement was significantly degraded only when emitting from $\Psi = 0.63$. The confinement in the latter case might be increased by more precise alignment of the conducting boundary. Much longer confinement times, which will be discussed in a future publication, have been measured at stronger magnetic field, lower pressure, and with fewer insulating rods (needed to support the probes) present in the plasma.

One reason that the confinement time is roughly constant could be that there are stronger radial electric fields when emitting from off the magnetic axis. The potential must drop from the emitter bias to the potential at the edge of the

TABLE I. Confinement times: 200 V bias, nonconforming boundary, neutral pressure 2×10^{-8} Torr, and $B = 0.02$ T.

Ψ_{emitter}	τ (ms)
0.0	3.6 ± 1.1
0.13	3.7 ± 1.1
0.33	6.0 ± 1.2
0.63	3.9 ± 1.6

TABLE II. Confinement times: 100 V bias, conforming boundary, neutral pressure 5×10^{-9} Torr, and $B = 0.02$ T.

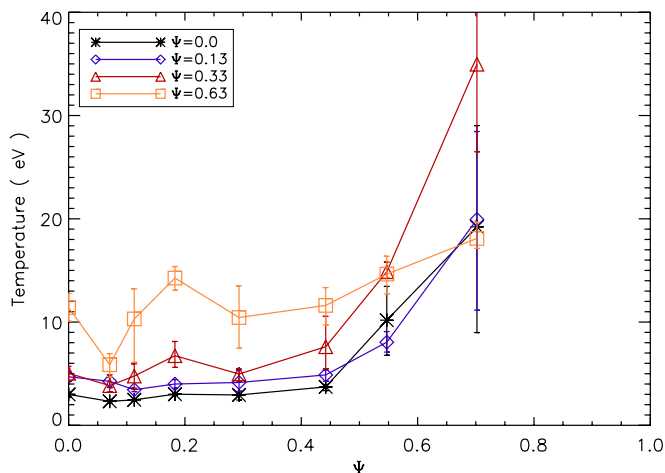| Ψ_{emitter}	τ (ms)
0.0	3.2 ± 0.5
0.13	3.0 ± 0.4
0.38	4.0 ± 0.8
0.63	0.18 ± 0.04

FIG. 9. (Color online) Temperature profiles when emitting at different off-axis positions with the conforming conducting boundary condition. The temperature across the inner surfaces is roughly constant, but the level increases with emitter position.

plasma over a shorter distance when the emitter is off axis, thus the electric field increases in proportion to the emitters distance from the axis. The $E \times B$ rotation closes bad orbits. A stronger rotation would be more effective thereby improving confinement.

V. NUMERICAL RESULTS

The experimental measurements are qualitatively consistent with the surfaces inside the location of the emitter being in a state of cross-surface thermal equilibrium and inconsistent with the other models that were considered. Numerical reconstructions of the equilibrium were done in order to show more clearly whether cross-surface thermal equilibrium is consistent with the experimental measurements.

Because the temperature is usually constant on the inner surfaces, whether the emission is at the axis or not, the main objective of numerical reconstructions is to compare the results for different $N(\Psi)$ profiles. $N(\Psi)$ is defined implicitly by Eq. (1) and is related to potential, temperature, and density by

$$N(\Psi) = n_e \exp\left(\frac{-e\Phi}{T_e(\Psi)}\right). \tag{7}$$

Using the equilibrium code described in Ref. 23 to solve Eq. (1), the procedure was: (1) Determine whether on-axis emission leads to equilibria that are consistent with cross-surface thermal equilibrium. It will be shown that they are not consistent. (2) Determine whether off-axis emission leads to equilibria that are consistent with cross-surface thermal equilibrium. It will be shown that they are consistent. (3) Having established that the on-axis emission is not consistent with cross-surface thermal equilibrium we determine that a $\log[N(\Psi)]$ profile fits the on-axis data very well. (4) Finally, we show that the $\log[N(\Psi)]$ profile does not fit the off-axis emission data, which shows that the profiles are clearly distinguishable from on-axis emission profiles.

Here we present, in detail, the analysis of the particular case when the emitter is at $\Psi = 0.63$ and there is no conducting boundary. The analysis of the other emitter positions and boundary conditions followed the same procedures and the results are consistent with this example.

In the results that follow $N(\Psi)$ is normalized by its value at the magnetic axis $N(0)$ and is denoted by $S(\Psi)$. In the reconstructions the zero of potential is defined at the axis at the toroidal location where the probe is located in the experimental results, so $N(0) = n_{e,0}$, which is the density at that location where $\Phi = 0$,[23]

$$S(\Psi) \equiv \frac{N(\Psi)}{N(0)} = \frac{n_e}{n_{e,0}} \exp\left(\frac{-e\Phi}{T_e(\Psi)}\right). \tag{8}$$

The thermal equilibrium condition was imposed by fixing the $S(\Psi)$ parameter to a constant value out to the Ψ location of the emitter, $\Psi = 0.63$. For Ψ values beyond the location of the emitter an exponentially decreasing function of Ψ was used. The temperature was set to be a constant with magnitude given by the weighted mean of the measurements on the inner surfaces. The PBS code also requires the Debye length to be specified at some point in the plasma. This
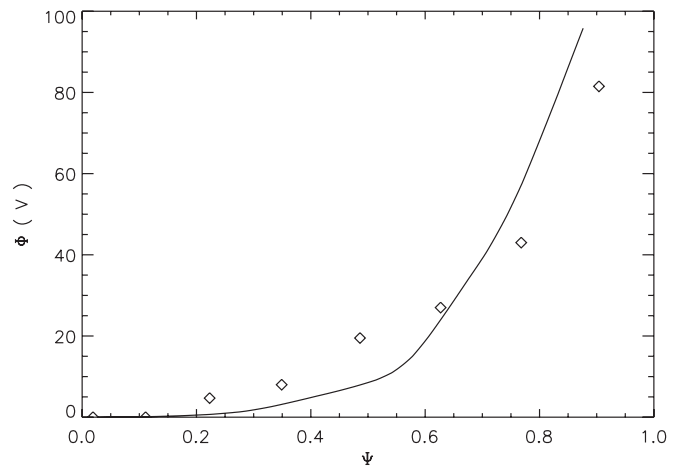

FIG. 10. Comparison of potential data from on-axis emission to a reconstruction with thermal equilibrium imposed to $\Psi = 0.63$. This solution is a poor fit to the measured data, which implies cross-surface thermal equilibrium is inconsistent with emission from the magnetic axis.

Debye length, $\lambda_{D,0}$, was specified at the location of the innermost probe. It was fine tuned, within experimental uncertainties, to yield the correct overall potential drop across the plasma. As long as the Debye length is much smaller than the minor radius, as is always the case for these cases, adjusting the Debye length only affects the scale of the numerically calculated potential and not the detailed agreement or disagreement between the numerical and measured potential profiles.

Imposing a constant $S(\Psi)$ profile and comparing to the on-axis emission data show that the cross-surface thermal equilibrium condition does not produce a good fit to the measured data (Fig. 10). The scaling of the potential is correct with the numerical reconstruction matching points on both the inner and outer surfaces. However, the reconstruction misses many of the points in the center by a significant margin.

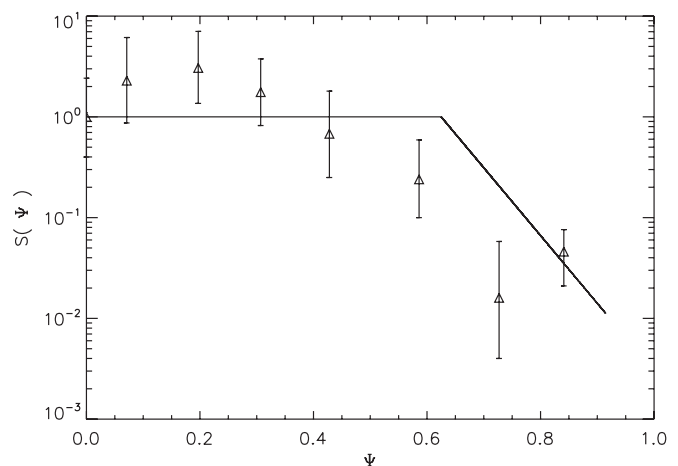The constant $S(\Psi)$ profile (Fig. 11) leads to a numeri-

FIG. 11. A constant $S(\Psi)$ profile out to the location of the emitter, in this case $\Psi = 0.63$, was used to calculate a potential profile that matches the experimental data from off-axis emission. Also shown on this plot are the values of $S(\Psi)$ calculated from experimental data, which are roughly consistent with the input to the reconstruction.
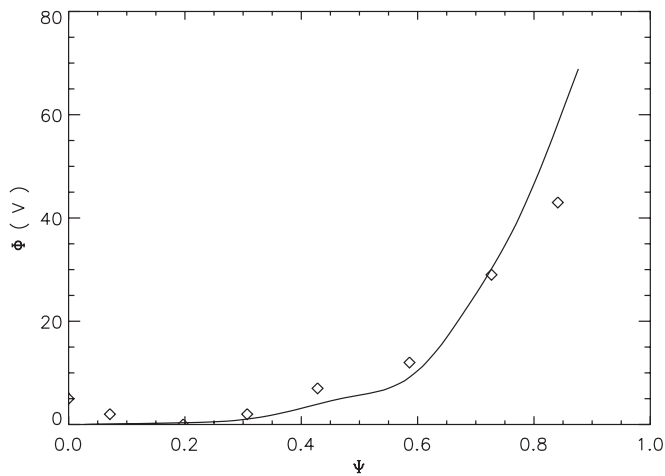
FIG. 12. Potential profile for the reconstruction with thermal equilibrium imposed to $\Psi=0.63$. This numerical solution is a reasonably good fit to the data.

FIG. 14. Potential profile for the reconstruction of on-axis emission showing good agreement with plasma potential measurements.

cally calculated potential profile that is a reasonably good fit to the data from off-axis emission (Fig. 12). The values of $S(\Psi)$ calculated from the experimental data are also consistent with a uniform value across the inner surfaces. Discrepancies, especially those at the edge, are probably due to approximations for the boundary conditions used in the reconstruction code.

To determine the $S(\Psi)$ profile when emitting at the magnetic axis, the $S(\Psi)$ profile was manipulated until the output potential profile matched the experimental data. The resulting $S(\Psi)$ profile was roughly parabolic in $\log(S)$. The profile was smoothed by fitting a quadratic function to $\log(S)$ and setting the innermost surfaces ($\Psi<0.15$) to a constant value to remove any artificial gradients at the axis (Fig. 13). The differences between the numerically calculated potentials using the smoothed function compared to using the nonsmoothed version were negligible. There is evidently some latitude in the choice of $S(\Psi)$, however, one can conclude that a quadratic $\log[S(\Psi)]$ profile accurately repro-
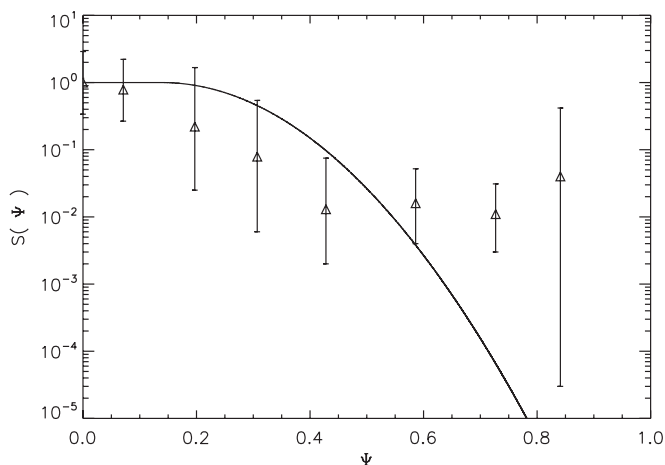

FIG. 13. This parabolic $\log[S(\Psi)]$ profile (solid line) produces a good fit to the plasma potential data for on-axis emission. Also shown are experimental values of $S(\Psi)$, which are roughly consistent with the input used in the numerical reconstruction.
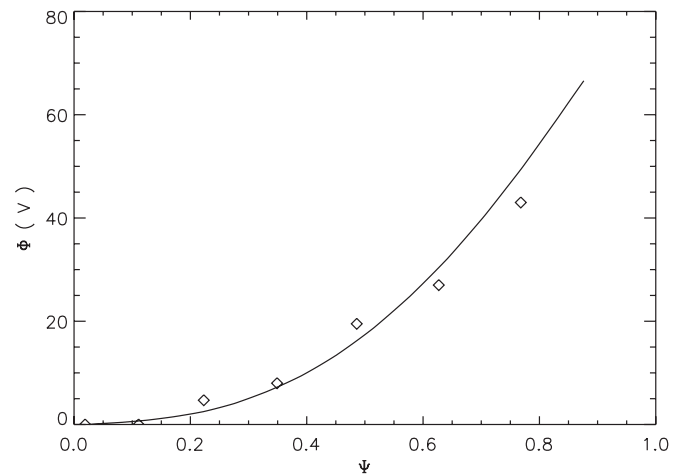
duces experimental data from on-axis emission (Fig. 14). The values of $S(\Psi)$ calculated from the experimental data also show profile that is radially decreasing and is roughly consistent with the parabolic profile used in the numerical reconstruction away from the plasma edge.

There is a small region of inner surfaces out to $\Psi\approx0.2$, where $S(\Psi)$ is nearly constant. This means that there is a volume of inner surfaces consistent with cross-surface thermal equilibrium even when emitting from the magnetic axis. Some volumes of thermal equilibrium are required by the boundary condition that there be no gradient in $S(\Psi)$ across the axis. Emitting from further off the magnetic axis can greatly expand this region.

Finally, we investigated whether an on-axis type $S(\Psi)$ profile can be used to reproduce plasma potential data from the off-axis emission case. The quadratic $\log[S(\Psi)]$ profile (Fig. 13) was used for these reconstructions. The quadratic profile cannot be used to produce a numerical potential profile that matches the data as well as the flat $S(\Psi)$ profile does. Figure 15 shows two examples with different scalings ($\lambda_{D,0}$). One scaling matches the potentials on the inner surfaces and the other matches on the outer surfaces. No scaling exists that can fit data points across the whole plasma for this $S(\Psi)$ profile.

The numerical reconstructions show that data from off-axis emission is consistent with cross-surface thermal equilibrium across the inner surfaces to the radial location of the emitter. There is a small region close to the axis that is consistent with cross-surface thermal equilibrium even for on-axis emission. The cross-surface thermal equilibrium region expands to the emitter location when emitting further from the magnetic axis. The reconstructions have also established that the consistency is a nontrivial one by showing that the on-axis equilibria are inconsistent with $N(\Psi)$ profiles that indicate thermal equilibrium out to $\Psi=0.63$ and that emission from $\Psi=0.63$ is inconsistent with the shape of the $N(\Psi)$ profile that best fits the on-axis emission data. These conclusions are true for all the different emitter locations and boundary conditions that were studied.
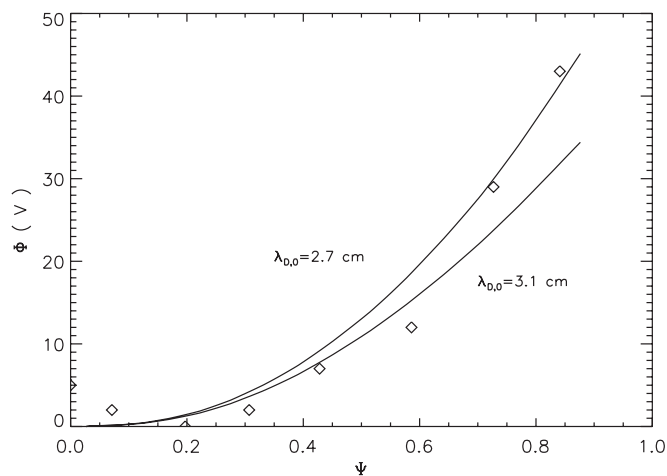
FIG. 15. Comparison of potential data from emission at $\Psi = 0.63$ with numerical reconstruction using a scaled parabolic $\log(S)$ profile. Two values of the Debye length parameter are used. Both are consistent with the experimental estimate of the Debye length, which has a 1σ range of 1.3–3.7 cm. The Debye length is expected to be longer than the typical 1.5 cm Debye length because the plasma at the axis when emitting off axis is relatively less dense. This numerical solution is a poor fit for any value of the parameter $\lambda_{D,0}$. This type of $S(\Psi)$ profile is therefore inconsistent with off-axis emission.

VI. DISCUSSION

Flat temperature profiles across the inner surfaces are a feature of CNT plasmas independent of the location of the emitter. When the emitter is at the axis, the flat temperatures imply that the thermal energy confinement is much lower than the particle confinement. When the emitter is not on the magnetic axis, we observe that the equilibrium of the inner surfaces not only features a flat temperature profile, but also a flat $N(\Psi)$ profile out to the location of the emitter, indicating that not only is the temperature constant but there is thermodynamic equilibrium across the surfaces internal to the emitter. In the Penning trap with an equipotential cathode[8] the electrons are emitted from an equipotential emitter, which intersects the magnetic field lines so that they are effectively connected. In a similar way, the thermal equilibrium across magnetic surfaces is equivalent to the equilibrium one would have if there was no magnetic field or a stochastic magnetic field in that volume. The electron plasma is relaxed, given the boundary condition set by the surface where the emitter is located.

The equilibrium described is distinct from the thermal equilibria that are observed in Penning traps. In the Penning trap global thermal equilibria exist under the constraint of conserved angular momentum. The plasma can relax thermodynamically without forming a hollow density profile because the angular momentum conservation acts as a potential well.[5] In CNT angular momentum is not conserved and the plasma is confined on the surfaces outside the thermal equilibrium region.

Equilibrium measurements are consistent with a thermal equilibrium spatial distribution of electrons across the inner surfaces even though the measured confinement time is not long compared with the estimated electron-electron collision time. This is consistent with previous results that showed that parallel electron distribution function is Maxwellian[13,20] and that the potential and density variation along the magnetic axis are consistent with the Boltzmann density variation predicted from thermodynamic equilibrium[21,24] for the same situation of confinement time on the same order as the like particle collision time. The underlying transport mechanism is not understood, however, the plasma satisfies the condition that the Larmor radius is much smaller than the Debye length, $r_L \ll \lambda_D$. In Penning traps long range guiding center collisions describe transport in this regime, which is must faster than predicted by the classical theory.[1,25] The same process could produce a much larger effective collision frequency in CNT as well.

The step size is determined by the deviation of drift trajectories from the magnetic surfaces. Two effects contribute to these deviations, the variation in potential on the magnetic surfaces ($\delta\Phi/\Phi$) and the ratio of the gradient and curvature drift speeds to the $E \times B$ drift, which closes the particle orbits. When emitting off-axis $\nabla\Phi$ on the inner surfaces is greatly reduced. This situation could produce large orbits that traverse the inner region. At the same time the overall confinement time from off-axis emission is roughly the same as from on-axis emission. It is possible that there is fast transport across the inner surfaces, which helps the inner surfaces to come to thermal equilibrium with each other while the plasma is confined by the slow transport across the outer surfaces. Our observations are all consistent with a situation where the confinement time is low in the inner regions, increases on the outer surfaces to $\Psi \approx 0.6$, then drops abruptly. A numerical study of particle orbits is being done and will be reported in a future publication.

Simple thermodynamic arguments predict cross-surface thermal equilibrium. Large particle orbits might occur, but are not necessary for the inner surfaces to be in cross-surface thermal equilibrium. For off-axis emission there is no source of electrons inside the emission surface. Even if there is good confinement in that region, the steady state situation must be a balance between diffusion into that region, subject to energetic constraints, and the loss of electrons from that region. This is the constant $N(\Psi)$ situation we observed. We observed that the temperature across the inner surfaces is a constant whether the emitter is located on-axis or off-axis, so no additional mechanism is needed to produce constant temperatures when emitting off-axis.

VII. CONCLUSION

When emitting from off the magnetic axis the balance between electrons entering the inner surfaces and the loss from the inner surfaces combined with a constant temperature is expected to lead to cross-surface thermal equilibrium. The constant temperature is the result of low thermal energy confinement relative to particle confinement and has been observed for plasmas created from on axis or off axis emission. Equilibrium measurements of pure electron plasmas created by emission from a heated biased filament off the magnetic axis show flat temperature profiles and plasma potential profiles in which the potential becomes more negative than the emitter bias on the inner surfaces. Analytic solutions

to the Poisson–Boltzmann equation in a simplified geometry show that the same characteristics would be observed if the inner surfaces are in a cross-surface thermal equilibrium. Numerical equilibrium solutions were then used to demonstrate that the experimentally observed equilibrium is consistent with thermal equilibrium across the inner surfaces.

There is a small volume of the innermost surfaces that appear to be in cross-surface thermal equilibrium even when the emitter is on the axis. Emitting from outside these surfaces expands the thermal equilibrium volume to the position of the emitter.

Estimates of the confinement time for off-axis equilibrium show that the confinement time is comparable to that with on-axis emission. At the same time there might be fast transport across the inner surfaces if the slow $E \times B$ rotation does not close the drift orbits in that region.

ACKNOWLEDGMENTS

[1] C. F. Driscoll, J. H. Malmberg, and K. S. Fine, Phys. Rev. Lett. **60**, 1290 (1988).
[2] T. M. O'Neil, Phys. Fluids **23**, 2216 (1980).
[3] T. M. O'Neil and C. F. Driscoll, Phys. Fluids **22**, 266 (1979).
[4] T. M. O'Neil and D. H. E. Dubin, Phys. Plasmas **5**, 2163 (1998).
[5] R. C. Davidson, *Physics of Nonneutral Plasmas* (Imperial College Press, London, 2001).
[6] T. S. Pedersen, J. P. Kremer, R. G. Lefrancois, Q. Marksteiner, N. Pomphrey, W. Reiersen, F. Dahlgreen, and X. Sarasola, Fusion Sci. Technol. **50**, 372 (2006).
[7] T. S. Pedersen and A. H. Boozer, Phys. Rev. Lett. **88**, 205002 (2002).
[8] C. F. Driscoll and J. H. Malmberg, Phys. Fluids **19**, 760 (1976).
[9] H. Himura, H. Wakabayashi, Y. Yamamoto, M. Isobe, S. Okamura, K. Matsuoka, A. Sanpei, and S. Masamune, Phys. Plasmas **14**, 022507 (2007).
[10] H. Himura, H. Wakabayashi, M. Fukao, M. Isobe, S. Okamura, and H. Yamada, IEEE Trans. Plasma Sci. **32**, 510 (2004).
[11] H. Himura, H. Wakabayashi, M. Fukao, and Z. Yoshida, Phys. Plasmas **11**, 492 (2004).
[12] H. Himura, H. Wakabayashi, M. Fukao, M. Isobe, S. Okamura, and H. Yamada, J. Plasma Fusion Res. **6**, 756 (2004).
[13] J. P. Kremer, T. S. Pedersen, R. G. Lefrancois, and Q. Marksteiner, Phys. Rev. Lett. **97**, 095003 (2006).
[14] L. D. Landau and E. M. Lifshitz, *Statistical Mechanics Part 1* (Elsevier, New York, 1980).
[15] R. D. Coalson and A. Duncan, J. Chem. Phys. **97**, 5653 (1992).
[16] E. S. Reiner and C. J. Radke, J. Chem. Soc., Faraday Trans. **86**, 3901 (1990).
[17] D. A. McQuarrie, *Statistical Mechanics* (University Science Books, Sausalito, 2000).
[18] P. L. Sachdev, *A Compendium on Nonlinear Ordinary Differential Equations* (Wiley, New York, 1997).
[19] T. S. Pedersen, J. P. Kremer, R. G. Lefrancois, Q. Marksteiner, X. Sarasola, and N. Ahmad, Phys. Plasmas **13**, 012502 (2006).
[20] J. P. Kremer, T. S. Pedersen, Q. Marksteiner, R. G. Lefrancois, and M. Hahn, Rev. Sci. Instrum. **78**, 013503 (2007).
[21] M. Hahn, T. S. Pedersen, Q. Marksteiner, and J. W. Berkery, Phys. Plasmas **15**, 020701 (2008).
[22] P. W. Brenner, T. S. Pedersen, J. W. Berkery, Q. R. Marksteiner, and M. Hahn, IEEE Trans. Plasma Sci. **36**, 1108 (2008).
[23] R. G. Lefrancois, T. S. Pedersen, A. H. Boozer, and J. P. Kremer, Phys. Plasmas **12**, 072105 (2005).
[24] R. G. Lefrancois and T. S. Pedersen, Phys. Plasmas **13**, 120702 (2006).
[25] D. H. E. Dubin, Phys. Plasmas **5**, 1688 (1998).